Earth and Planetary Science Letters 500 (2018) 192–204

Contents lists available at ScienceDirect

Earth and Planetary Science Letters

www.elsevier.com/locate/epsl

Dynamics of Mount Nyiragongo lava lake inferred from thermal imaging and infrasound array

Sébastien Valade [a,*], Maurizio Ripepe [a], Giovanni Giuffrida [b], Katcho Karume [c], Dario Tedesco [d,e]

[a] Dipartimento di Scienze della Terra, Università di Firenze, Florence, Italy
[b] Institute Nazionale Geofisica e Vulcanologia, Palermo, Italy
[c] Observatoire Volcanologique de Goma, 142, Avenue du Rond-Point, Quartier des Volcans, Goma, Democratic Republic of the Congo
[d] DISTABIF, Campania University – Luigi Vanvitelli, 81100 Caserta, Italy
[e] JOC, UN-MONUSCO, UN-Goma, Democratic Republic of the Congo

ARTICLE INFO

Article history:
Received 16 April 2018
Received in revised form 1 August 2018
Accepted 2 August 2018
Available online xxxx
Editor: T.A. Mather

Keywords:
lava lake
Nyiragongo
thermal imaging
infrasound array
magma convection

ABSTRACT

Lava lakes provide a direct observation window into processes which usually remain hidden, such as magma convection and outgassing dynamics. We here report a coupled analysis of thermal infrared footage and infrasound array recordings at Mount Nyiragongo (D. R. Congo), and derive a conceptual model of the lava lake's convective system and outgassing mechanism. We suggest that surface flow results from a horizontal pressure gradient at the surface of the lake, driving the crust from high-pressure regions where hot upwelling magma impinges the surface, to low-pressure regions where cold downwelling magma pulls away from the surface. The ascending current of this convection cell carries gas pockets, which once at the surface, are dragged across the lake into downwelling sinks. Such sinks are characterized by persistent chaotic bubble bursting (spattering), whose intensity and position are tracked from infrasound array analysis. Fluctuations of these are observed, but have not been correlated with oscillations of the lava lake level, nor with the variations of surface velocities, both recorded from infrared footage. We also report the activity of a new eruptive vent, which opened early 2016 near an inner circular fracture of the crater's third terrace. We show that the vent's activity was intermittent, alternating between explosive strombolian activity and effusive activity. The latter produced lava flows which spread on the crater's last terrace before cascading into the active lava lake. Although no significant change in the lake behavior was witnessed while the new eruptive vent was active, increased attention should be addressed as this new activity could reflect over-pressurization of the shallow magmatic system. The variety of phenomena captured by this study complements and expands observations reported at other low-viscosity lava lakes, chiefly Kilauea (Hawai'i) and Erta Ale (Ethiopia). Despite Nyiragongo's more vigorous convective regime (where multiple convective cells can operate simultaneously), we suggest that the mechanisms controlling the surface motion and outgassing are similar at all three systems, pointing to generic processes governing the dynamics of low-viscosity lava lakes.

1. Introduction

Active lava lakes are the exposed, uppermost part of volcanic plumbing systems (e.g., Tazieff, 1994). As such, they provide a direct window into what is usually hidden at other open-vent volcanoes, in particular magma convection and outgassing dynamics. Nyiragongo volcano (Democratic Republic of Congo) is famous for hosting the world's largest persistently active lava lake (e.g., Burgi et al., 2014; Patrick et al., 2016b). The first expeditions into the crater were carried in 1958 and 1959 (de Magnée, 1959; Evrard, 1960), during which were deployed a spectacular variety of sensors: photographic cameras, spectrographs, seismographs, pyrometric probes, optical pyrometers, magnetometers, Geiger–Muller counters, theodolites, as well as gas and lava sampling devices. Although the lava lake size, shape, and elevation were significantly different from today, the collected data provide the first quantitative descriptions of the lava lake behavior which are still relevant as of today: estimates of plate horizontal speeds (0.25 m/s), lake level oscillations (cyclic meter-scale oscillations, and sudden deca-metric drops), magma temperatures (>950 °C at 1 m depth),

* Corresponding author. Now at Dep. Computer Vision & Remote Sensing, Technische Universität Berlin, Berlin, Germany.
E-mail address: valade.sebastien@gmail.com (S. Valade).

https://doi.org/10.1016/j.epsl.2018.08.004
0012-821X/

thermal budget (0.96 GW), volcanic micro-seismicity ("volcanic tremor", 0.1–0.5 s period), etc. Since then, and despite the difficulty of carrying out field work in a politically unstable region, a number of other measurement campaigns have been undertaken to investigate: 1) degassing rates and chemistry (e.g., Arellano et al., 2017; Barrière et al., 2017; Bobrowski et al., 2016; Sawyer et al., 2008), 2) heat budget (e.g., Le Guern, 1987; Spampinato et al., 2013), 3) lake level fluctuations (Burgi et al., 2014; Smets et al., 2016), 4) petrography (e.g., Platz et al., 2004), and extensive literature on various aspects of the 1977 and 2002 flank eruptions (e.g., Carn, 2002; Giordano et al., 2007; Komorowski et al., 2002; Tazieff, 1977; Tedesco et al., 2007; Wauthier et al., 2012). These studies have contributed to the general understanding of lava lakes, which still remains predominantly informed by investigations on other lakes, such as Kilauea (Hawai'i), Erta Ale (Ethiopia) and Erebus (Antarctica) (see Patrick et al., 2016b for an overview).

Our experiment took place between 19–23 April 2016, shortly after it was reported by the Volcanological Observatory of Goma (OVG) that a new eruptive vent opened on 29 February 2016, inside the crater next to the existing active lava lake (Balagizi et al., 2016). We deployed an infrasound array inside the crater, and here report on the infrasonic recordings of both the lava lake and the new eruptive vent. In addition, thermal video recordings were undertaken to investigate the kinematics of lake surface (horizontal and vertical motions), which enable us to derive a conceptual model of the lake convective system and outgassing mechanism. Lastly, from the combined thermal and dynamical analysis we derive a dimensionless analysis, in an attempt to parametrize the lake thermodynamical behavior, and thereby allow quantitative comparison with other natural and experimental convective systems.

2. Volcanic activity

The observed volcanic activity was characterized by two distinct features: (i) the active lava lake, confined within a pit crater on platform P3, and (ii) a recently opened eruptive vent, close to the eastern wall of platform P3 (Fig. 1, Supplementary Video 1). During our field work, the lake was ~55 m below the level of platform P3, in a slightly elliptical pit with dimensions of 235 × 255 m (N–S and E–W axes respectively). The lake itself had slightly smaller dimensions, of approximately 200 × 230 m (~36,000 m^2). The molten lava is covered by a cooled black crust, organized in a mosaic of plates which glide from regions of upwelling (where crust is generated) to regions of downwelling (where crust is consumed). The regions where crust is recycled most intensively are regions of continuous spattering, characterized by sustained bubble bursting, whose position move continuously across the lake surface.

The new vent on the other hand was first witnessed by the OVG on 29 February 2016. The eruptive activity started from an inner circular fracture close to the eastern wall of platform P3, building up in nearly two months a 30 m-high spatter cone. The activity of the new vent was intermittent, and characterized by distinctive cycles. The activity started with weak gas emission, regularly interrupted by loud explosions with no ejection of magma. Progressively, these explosions erupted fresh lava which mostly remained on the slopes of the newly forming cone. As the rate and intensity of these explosions increased, the explosions became nearly continuous, forming a small lava-fountain several meters high. At this point magma started overflowing from the cone, feeding a lava flow which spread onto platform P3 before cascading into the lava lake (Fig. 1).

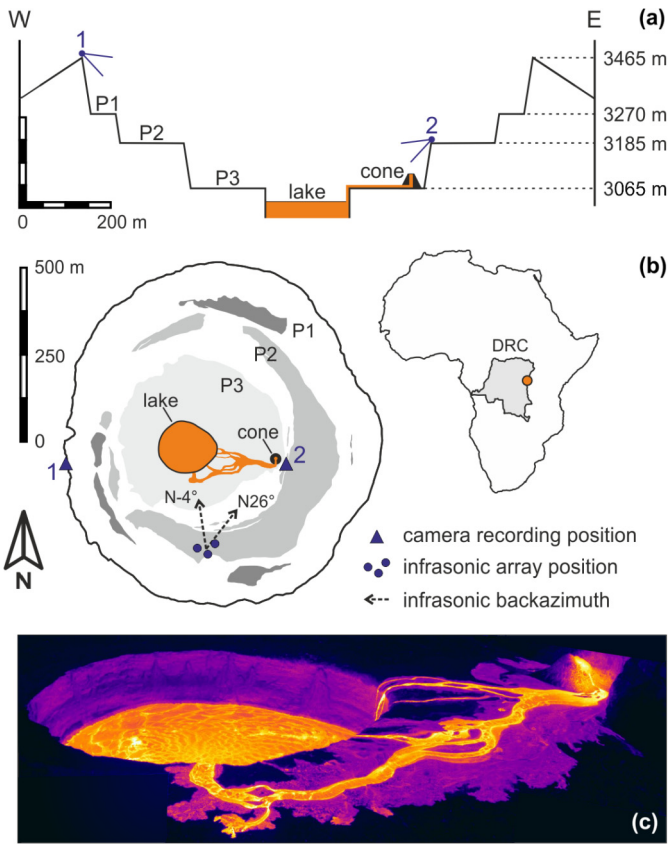

Fig. 1. (a) Schematic cross section of Mount Nyiragongo. The three platforms are referred as P1, P2 and P3, the active lava lake being confined in a pit crater on P3. Altitudes were taken accordingly with Smets et al. (2016), except for P2 for which GPS measurement was taken during the campaign. (b) Map of Mount Nyiragongo and position of the infrasound array and thermal infrared recordings position (labeled 1 and 2, on the crater rim and platform P2 respectively). The arrows 26°N and −4°N point to the two main sources of infrasound, corresponding respectively to the spatter cone and the lava lake (Fig. 8d). The outlines of the platforms and lake are from a WorldView 1 image from January 29, 2010. Note however that the lake extent fluctuate slightly with the changes of the lake level within the pit crater. (c) Thermal infrared image taken on 2016-04-20 21:35 GMT, from a position close to the infrasound array.

3. Methods

An infrasound array was deployed to record the infrasonic activity during the 2-day experiment (20–22 April 2016). The array consisted of 3 pressure sensors (2 ITEM sensors 0.01–300 Hz sensitivity, 1 OMEGA sensor 0.001–100 Hz sensitivity, 100 Hz sampling rate), installed on platform P2 in a 50 m-wide triangular aperture configuration (Fig. 1). Array analysis by a multichannel semblance and grid-searching procedure was performed, allowing for discrimination of coherent signal in terms of propagation back-azimuth and apparent velocity (Ripepe and Marchetti, 2002). In doing so, infrasound coming from the lava lake and from the spatter cone could be distinguished.

In addition, thermal infrared videos were temporarily recorded (FLIR SC660 camera, 7.5–14 µm spectral range, 640 × 480 pixel, 24° × 18° lens field of view) to estimate heat fluxes and follow the eruptive dynamics. Measurements of the lake were carried from both the crater rim and from platform P2 (positions 1 and 2 in Fig. 1). Corrections for emissivity and atmospheric effects were performed using the software *FLIR ThermaCam Researcher*, which uses the LOWTRAN atmospheric model. Here, emissivity was set to 0.96, relative atmosphere humidity to 55%, atmosphere temperature to 10 °C, and slant distance-to-target to 660 m and 475 m

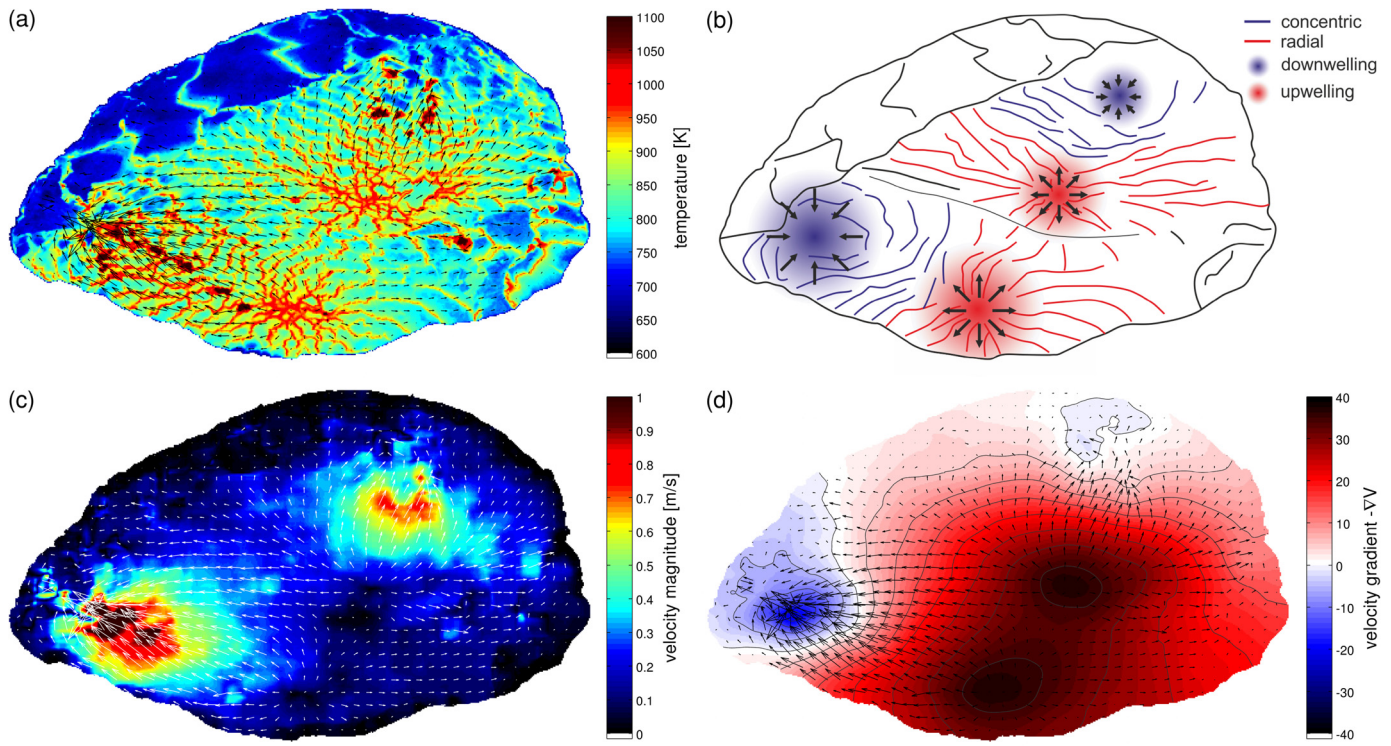

Fig. 2. Thermal infrared recording and processing, taken on 2016-04-21 11:15:07 GMT (recording position 1). (a) Thermal infrared image. (b) Schema of plate boundaries: blue boundaries are concentric to the downwelling spots, red boundaries are radial to the upwelling center, and black boundaries are old and inherited from former convective structures not captured in the snap shot. (c) Velocity magnitude map. (d) Velocity gradient map $-\nabla V$. (For interpretation of the colors in the figure(s), the reader is referred to the web version of this article.)

for recording positions 1 and 2, respectively (taken as the distance from the camera to the lake center, see Appendix for image georeferencing). Lake-surface radiative power was estimated from the Stefan–Boltzmann formula $Q = \sigma \cdot \varepsilon \cdot \sum (T_i^4 \cdot A_i)$, where $\sigma = 5.67 \times 10^{-8}$ W·m^{-2}·K^{-4} is the Stefan–Boltzmann constant, ε the emissivity, T_i the surface temperature in Kelvin of pixel i, and A_i the area of the corresponding pixel in m^2. Lake-surface velocity and flow direction were calculated using the Farnebäck dense optical flow algorithm implemented in the *OpenCV* library. Image contrast was enhanced by computing the thermal radiation image (Q) which was then filtered with the Laplacian of Gaussian filter (5×5 window, 0.5 standard deviation). The vectors of motion expressed in image coordinates (pixels per frame) were converted to geographic coordinates (meters per frame) by projecting the image onto a horizontal plane representing the lava lake surface (see Supplementary Material for details). Lake depth below P3 was estimated from the projection of the image onto a vertical plane representing the pit wall. Len distortions effects were neglected, assuming a rectilinear geometry. Trajectories of traveling bubbling sources on the lake surface were tracked using the Lucas–Kanade sparse optical flow algorithm, also implemented in the *OpenCV* library.

4. Results

4.1. Lake surface motion

The lake surface consists of a mosaic of dark crustal plates, separated by narrow incandescent cracks (Fig. 2a). Plates move from regions of magma upwelling where crust is formed, to regions of downwelling where crust is consumed. Upwelling regions are characterized by diverging vectors of motion, indicating where magma rises to the surface, cools, and forms a thin crust which spreads radially (Fig. 2a, b). The incandescent cracks tend to be organized radially with respect to the spreading center (highlighted in red in Fig. 2b), designing elongated plates which are dislocated when surface crust velocity is increased, namely in the proximity of downwelling regions. Downwelling regions are characterized by converging plate motion, and refer to zones where crust is consumed. The downwelling process is either quiescent, where converging plates gently fold and sink into the lake, or vigorous, where chaotic bubble bursting (hereafter referred to as spattering) tears the crust to shreds. The highest surface crust velocities are recorded in the vicinity of spattering regions, where the acceleration of the plates becomes significant as they are drawn into the spattering site (Fig. 2c). This acceleration stretches and tears the crust, generating incandescent cracks concentric to the spatter source, as highlighted in blue in Fig. 2b (see also Supplementary Video 1). Zones caught in between two spatter zones are pulled apart, exposing incandescent lava which cools to form crust. This crust generation process is passive, in contrast to that resulting from magma upwelling.

In order to localize the upwelling and downwelling regions, we compute the velocity gradient ∇V, defined as $\nabla V = \partial V/\partial x + \partial V/\partial y$, where $u = \partial V/\partial x$ and $v = \partial V/\partial y$ are the horizontal and vertical velocity vectors components recovered from the optical flow analysis. The velocity gradient ∇V is thus obtained from the two-dimensional numerical integration of the matrices u and v. We define upwelling regions where $-\nabla V > 0$ (i.e., diverging vectors), and downwelling regions where $-\nabla V < 0$ (i.e., converging vectors), see Supplementary Material for details. In doing so, we are able to highlight upwelling and downwelling centers, and show that multiple centers may coexist simultaneously in the lava lake (Fig. 2d).

Plate motion appears as a complex interplay between two driving processes: (1) upwelling, pushing magma from depth towards the surface, and (2) downwelling, dragging surface crust towards spattering regions. Because multiple upwelling and downwelling

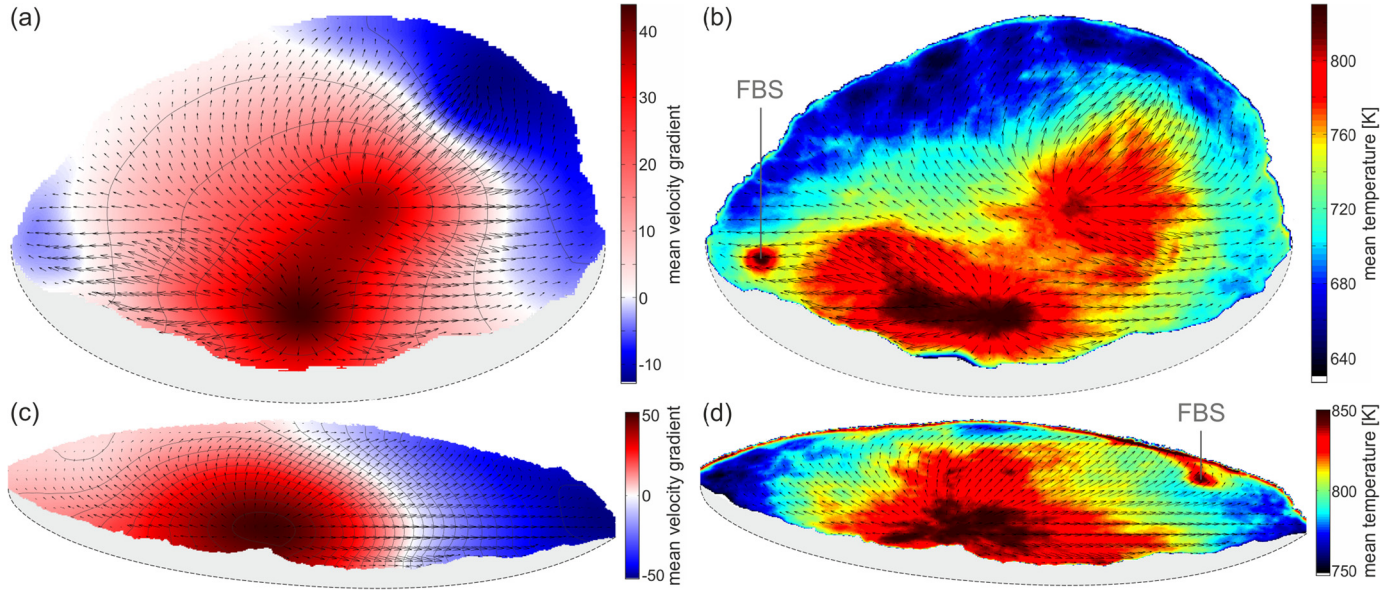

Fig. 3. Left column plots (a), (c) are average velocity gradient maps, right column plots (b), (d) are average temperature maps. Top row plots were acquired from the recording position 1, while the bottom row plots were acquired from recording position 2, as shown in Fig. 1. The spot labeled FBS (Fixed Bubbling Spot) refers to a stationary bubbling source, where large bubbles burst at regular time intervals. The area shaded in gray roughly indicates the obscured area of the lava lake which is not capture within the field of view.

centers may coexist, whose position shift and affect one another through time, the resulting surface motion is highly complex (Supplementary Video 2). In order to simplify the interpretation of the lava lake circulation, we filter out the short-term fluctuations of the lake motion, by computing the time-averaged temperatures and velocity gradients. The mean velocity gradient showed in Figs. 3a and 3c, clearly indicates that despite the complex surface motion, upwelling is on average positioned in the lake center, and downwelling along the lake margins. The mean lake temperatures on the other hand (Fig. 3b, d), highlights that upwelling corresponds to high temperature regions (resulting from thin and small crustal plates), whereas the downwelling regions along the lake margins are on average cooler.

Lake surface velocities are on average <1 m/s, as shown in the velocity histogram (Fig. 4a). Mean lake velocities correlate with mean lake temperatures, where high temperatures are associated with high velocities, and vice versa (Fig. 4a, b). On short time scales, oscillations of the surface velocity were observed with an average period of $\sim$80 s, mostly visible in the regions of downwelling (Fig. 4c). Oscillations were observed only when the lake motion reduces to only one upwelling and downwelling center.

4.2. Lake spattering activity

Spattering refers to sustained chaotic bubble bursting on the surface of the lava lake (e.g., Patrick et al., 2016a). Because the crust appears pierced by underlying gas bubbles, some authors have also defined this as “boiling activity” (Bobrowski et al., 2016), or as “lava fountaning” (e.g., Burgi et al., 2014). Spattering is most violent in regions where plates converge, i.e. where the velocity gradient is minimum (Fig. 2d). These regions behave as sinks, towards which the surrounding crust is dragged, and where it is shredded apart by persistent bubble bursting (Fig. 5a and Supplementary Video 4). The crust thus appears as a thin flexible skin, likely a few centimeters thick, which glides over the underlying incandescent lava. Together with the crust, multiple small bubbling spots scattered across the lake also get drained towards these spattering regions (Fig. 5b). As these get closer to the area of sustained spattering, they tend to align, merge, ultimately forming long alignments pointing towards the main spattering sink (Fig. 5a,

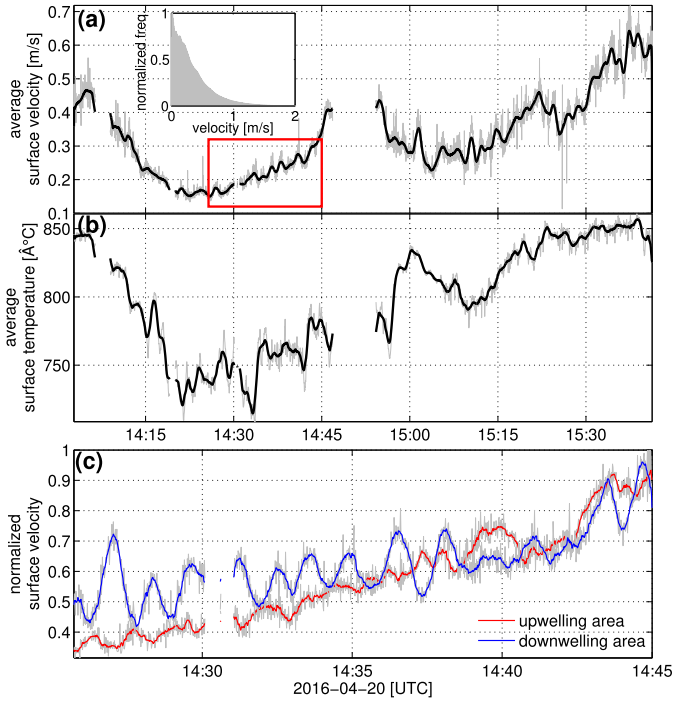

Fig. 4. (a) Average lake surface velocity and (b) average lake surface temperature, recorded from position 2. The histogram shown in the inset is the average histogram of the velocities recorded during the entire plotted period. The red box highlights the time span zoomed in plot c. (c) Velocity oscillations recorded in the downwelling and upwelling regions of the lake. The curves were obtained by averaging the surface velocities expressed in image coordinates of the pixels in areas of upwelling ($-\nabla V > 0$) and downwelling ($-\nabla V < 0$) respectively.

b). These alignments are in most cases parallel to the flow streamlines (i.e., tangent to the velocity vectors as in Fig. 5c), but can in some cases be perpendicular to the flow if spattering occurs at the junction between two upwelling centers (e.g., 11:38:30 UTC in Supplementary Video 2).

Tracing back the trajectory of the traveling bubbling sources across the lake, we show that they originate in two regions. Firstly,

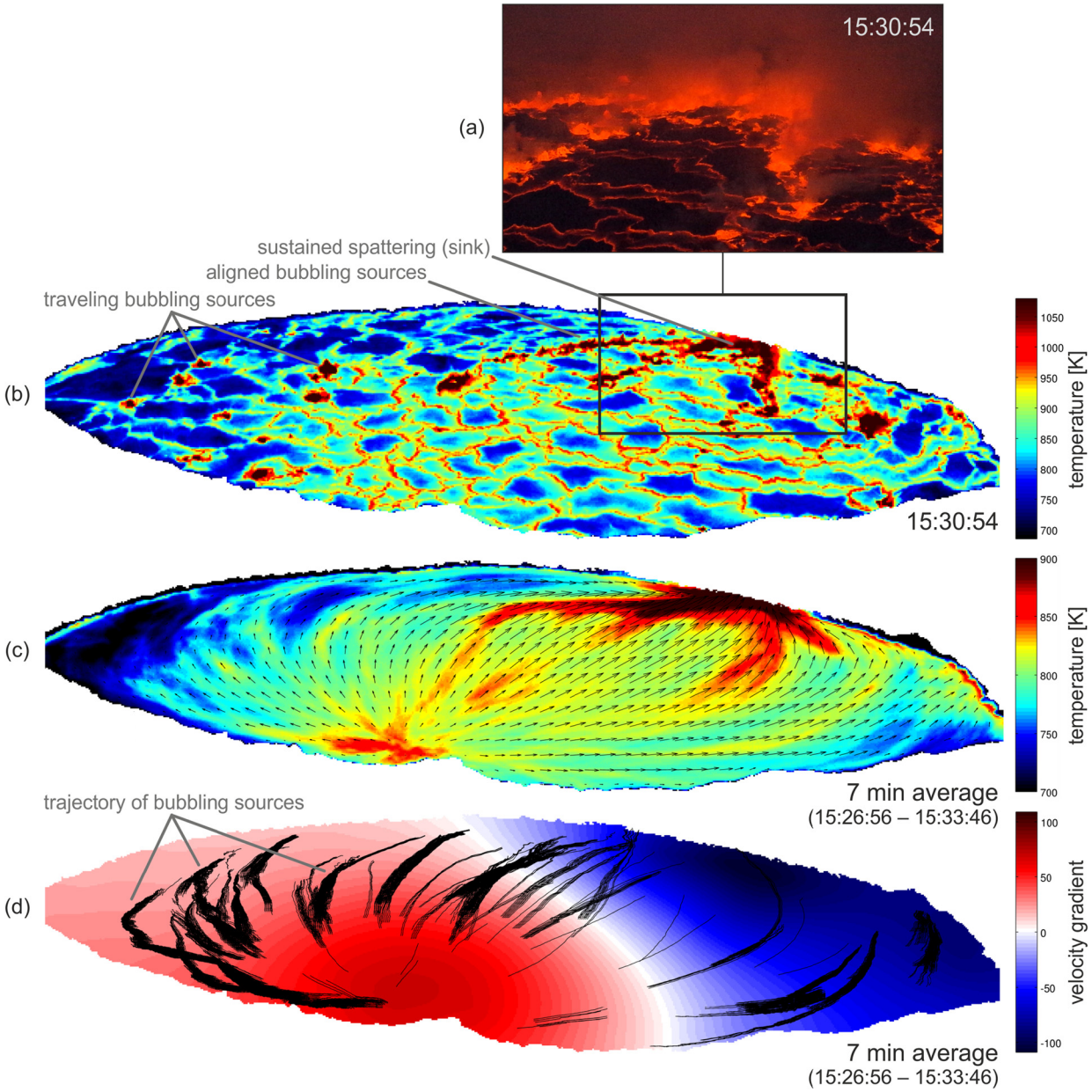

Fig. 5. Lava lake recordings taken on 2016-04-20 from recording position 2. (a) Optical imagery of the spattering sink and the aligned bubbling sources, corresponding to region highlighted by a black box in (b). Video footage of this zoomed area is provided in Supplementary Video 4. (b) Thermal infrared image. (c) Average temperature and velocity vectors over a 7-min period. (d) Average velocity gradient over a 7-min period, and trajectory of the traveling bubbling sources across the lake (see Supplementary Video 3).

in the vicinity of the spattering regions, where the crust is accelerated, stretched, and ultimately pierced by small bubbles which concentrate in the narrow cracks separating the plates. Secondly, near the upwelling regions, where the crust is thin and easily punctured by uprising gas pockets. Interestingly, their trajectories trace curved paths across the lake (Fig. 5d, and Supplementary Video 5) as the surface flow drags them into the downwelling region, recalling the helicoidal motion of a fluid drained by a sink. This observation strongly suggests that this bubbling dynamics, and spattering in general, is shallowly rooted.

Only in one specific spot close to the northern border of the lava lake, we observed a stationary bubbling source, where large bubbles burst at regular time intervals (every 15–30 s on average). It appears as a visible hot spot on the mean temperature maps of Fig. 3, labeled as FBS (Fixed Bubbling Spot). The fact that its position was stable regardless of the direction of the surface motion suggests that in this specific spot there is a stationary deep source of gas, from where bubbles rise independently of the convective cells. Similar sporadic, quasi-periodic bubble bursting separated by tens of seconds to minutes has been observed at Kilauea, usually clustered in the northern part of the lava lake (Patrick et al., 2018). At Erta Ale, large bubbles regularly breaking at a fixed position have also been reported (Bouche et al., 2010).

The lake spattering activity was observed during the entire recording campaign. The number and the position of the spattering sinks shifted continuously across the lava lake, but tended to be most stable in peripheral regions, eventually anchoring onto the lake margin (e.g., Fig. 5a, b). A coupled analysis of video and infrasonic recordings suggests that spattering is the main source of infrasound within the lava lake. On one hand, we tracked the position of the main spattering sink in the video footage as the velocity gradient minimum $\nabla V_{\min}$, and converted its geographical coordi-

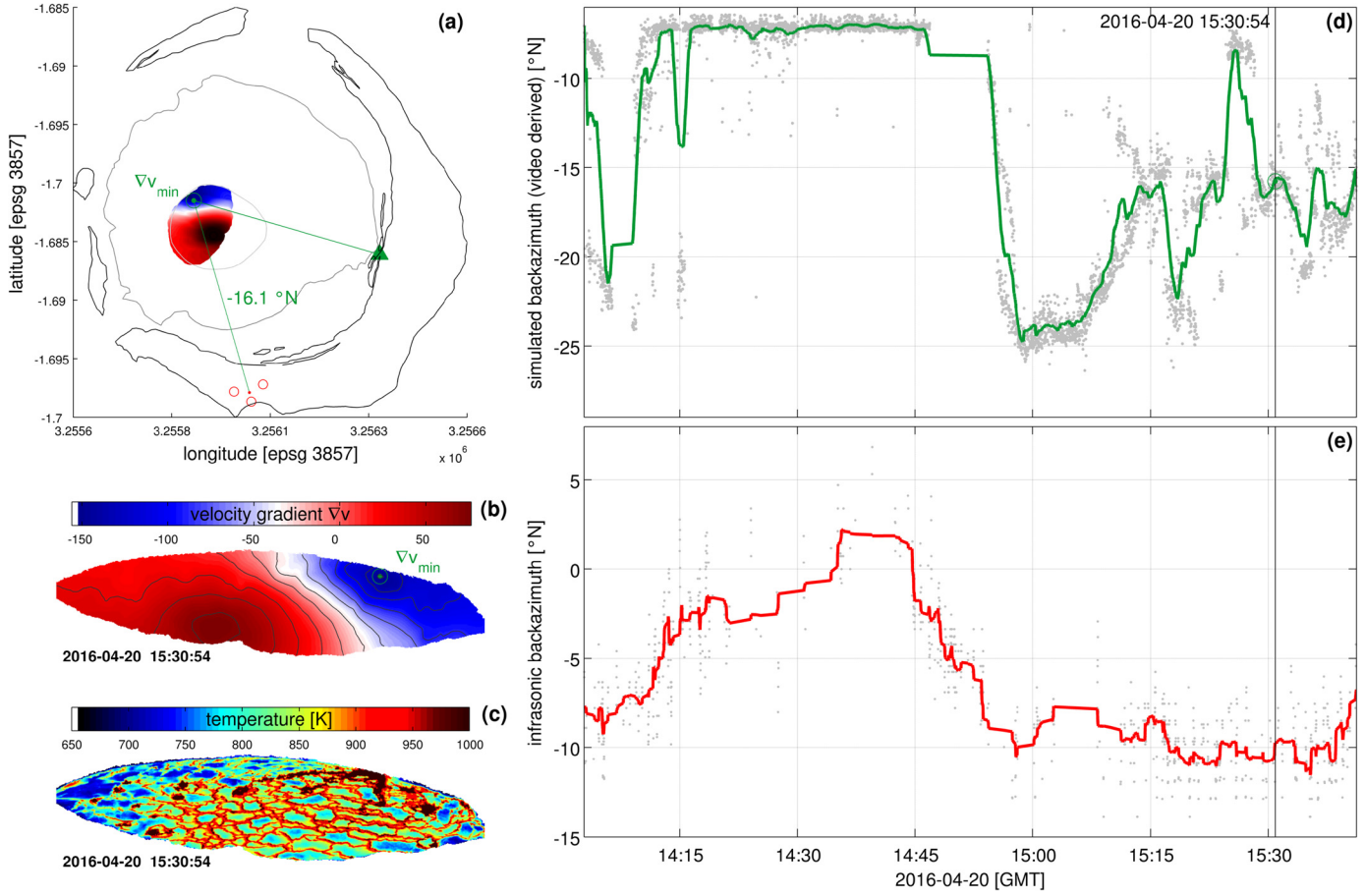

Fig. 6. Coupling of infrared video analysis and infrasonic records suggesting that spattering is the main source of infrasound within the lava lake. (a) Representation of how the downwelling sink $\nabla V_{\min}$ tracked in the camera data is converted from geographical coordinates (i.e., green spot on the lake) to polar coordinates centered on the array (i.e., dashed green line). The green triangle highlights the camera recording position, and the red circles the position of the 3 infrasonic sensors. (b) Gradient velocity map showed in plot a, and associated infrared image (c). (d) Azimuth of the downwelling sink recovered from the camera data. (e) Back-azimuth of infrasonic signal originated from the lava lake. The good agreement between (d) and (e) suggests that spattering generates the infrasonic signal coming from the lava lake.

nates into back-azimuth relative to the array (Fig. 6a, d). On the other hand, infrasonic detections coming from the lava lake were identified as those with back-azimuth <5°N (Fig. 6e, Fig. 8c). The fairly good agreement between the azimuth variations recorded by the array and by the camera (i.e., Fig. 6d and 6e respectively) suggests that spattering generates the infrasonic signal coming from the lava lake. Infrasound array analysis can thus be used to track both the intensity and the location of the spattering within the lava lake, both of which show clear fluctuations through time (respectively Fig. 8c and 8d, red symbols).

4.3. Lake level fluctuations

Small variations of the lava lake level were observed from infrared camera recordings. These were recorded from platform P2 (recording position 2), from where low camera inclination angle allowed best vertical resolutions. Lake level fluctuations are tracked by the vertical position of the lake surface in each column of pixels across the image width. In each frame of the video recording, we obtain for each column a time series of lake surface vertical coordinate in the image, which is then converted to relative vertical variations with respect to the first frame. By averaging the pixel time series, we obtain the mean vertical variations of the lake surface (respectively gray and red curves in Supplementary Video 6). Finally, we convert these variations from pixels to meters using an average pixel height value calculated from the projection of the image onto a vertical plane representing the pit wall (see Supplementary Material for details).

The resulting lake level fluctuations has a peak-to-peak variation of ∼1.6 m and a period of ∼1 hr (Fig. 7a). These fluctuations do not have any clear correlation with the surface velocity, radiative power, nor spattering intensity (Fig. 7b–d). However we point out that when the lake level is at its highest, the plate velocities and temperatures are low, and plate size are large (i.e., 14:20 GMT, Fig. 7 and Supplementary Video 3). Conversely, when the lava level is at its lowest, velocities increase together with the degassing activity (i.e., >14:30 GMT).

4.4. Lake thermal and dynamical characterization

The measured lake temperatures range between 600 K and 1250 K, which respectively correspond to the temperature of the cooled crust and that of the fresh lava (Table 1). The radiative power was estimated from the Stefan–Boltzmann formula described previously, and varied between ∼0.3–0.6 GW (Fig. 7) from recording position 2 (from where ∼50% of the lake surface was imaged, see Appendix), and between 0.6–0.8 GW from recording position 1 (from where ∼85–90% of the lake was imaged). These are in agreement with the values reported Spampinato et al. (2013) (0.6–1.1 GW).

In order to characterize the lava lake dynamics in a way that allows quantitative comparison with other natural and experimental systems, we compute dimensionless numbers commonly found in fluid mechanics literature. The most relevant ones which can help parametrize the fluid behavior are the Rayleigh, Reynolds, Prandtl, and Nusselt numbers. Although there is some uncertainty in their

Table 1
Physical properties and dimensionless numbers used to characterize the lava lake. Justification of the selected values, and details on the computation of dimensionless numbers can be found in the Supplementary Material.

Physical property	Symbol	Unit	Range	Value	Source
fluid density	ρ	$kg{\cdot}m^{-3}$	950–2800	1800	[1]–[2]
fluid dynamic viscosity	η	Pa.s	60–150	100	[3, 4]–[5]
fluid kinematic viscosity (a.k.a. momentum diffusivity)	$\nu = \eta/\rho$	$m^2{\cdot}s^{-1}$	5.7×10^{-2}–6.3×10^{-2}	5.5×10^{-2}	–
fluid thermal diffusivity	k	$m^2{\cdot}s^{-1}$	2.5×10^{-7}–7×10^{-6}	10^{-6}	[3]–[6]
fluid specific heat capacity	C_p	$J{\cdot}kg^{-1}{\cdot}K^{-1}$	1000–1150	1150	[6,2]–[5,7]
fluid thermal conductivity	$K = k \cdot \rho \cdot C_p$	$W{\cdot}m^{-1}{\cdot}K^{-1}$	1–3	2.07	[7, 2, 6]
thermal expansion coefficient	α	K^{-1}	3×10^{-5}–5×10^{-5}	4×10^{-5}	[9]–[5,7]–[2]
temperature magma	T_m	K	1370–1400	1380	[10,11,12,3]
temperature magma solidus	T_s	K	1200	1200	[7]
temperature lava	T_l	K	1100–1250	1150	measured
temperature crust	T_c	K	600–700	650	measured
temperature atmosphere above lake surface	T_a	K	300–360	330	[11, 13]
temperature difference between thermal boundaries driving the convection	$\Delta T = T_m - (T_a + T_s)/2$ $\Delta T \approx T_m - T_c$	K	–	615	–
temperature pixel	T_{px}	K	–	–	measured
surface emissivity	ε	–	0.55–0.97	0.96	[13,8,14]
Stefan–Boltzmann constant	σ	$W{\cdot}m^{-2}{\cdot}K^{-4}$	–	5.67×10^{-8}	–
fluid velocity	u	$m{\cdot}s^{-1}$	0.1–0.7	0.4	measured
characteristic length scale	D	m	10–100	50	measured
pixel area	A_{px}	m^2	–	–	calculated
radiative power	$Q = \sigma \cdot \varepsilon \cdot T_{px}^4 \cdot A_{px}$	W	300–600	500	measured
radiative flux	$Q_f = \sigma \cdot \varepsilon \cdot T_{px}^4$	$W{\cdot}m^{-2}$	1200–2200	2000	measured
Grashof number	$Gr = (g \cdot \alpha \cdot \Delta T \cdot D^3)/\nu^2$	–		9.8×10^6	calculated
Prandtl number	$Pr = \nu/k$	–		5.6×10^4	calculated
Rayleigh number	$Ra = (g \cdot \alpha \cdot \Delta T \cdot D^3)/(\nu \cdot k) = Gr \cdot Pr$			5.4×10^{11}	calculated
Reynolds number	$Re = (U \cdot D)/\nu = Pe/Pr$	–		360	calculated
Nusselt number	$Nu = (Q_f \cdot D)/(K \cdot \Delta T)$	–		79	calculated
Péclet number	$Pe = (U \cdot D)/k$			2×10^7	calculated

[1] Carbone et al., 2013; [2] Davaille and Jaupart, 1993; [3] Giordano et al., 2007; [4] Burgi et al., 2014; [5] Harris, 2008; [6] Karlstrom and Manga, 2006; [7] Patrick et al., 2004; [8] Spampinato et al., 2013; [9] Turcotte and Schubert, 2002; [10] Helz and Thornber, 1987; [11] Sawyer et al., 2008; [12] Le Guern, 1987; [13] Burgi et al., 2002; [14] Ball and Pinkerton, 2006.

estimation, the order of magnitude of these quantities should be considered for assessing dynamic similarity between systems (Table 1). Details on the computation of dimensionless numbers and on justification of the selected values can be found in the Supplementary Materials.

The Rayleigh number $Ra = Gr \cdot Pr$ is here used to quantify the vigor of convection resulting from thermally induced density variations in the fluid (Anderson, 2007). It is defined as the product of the Grashof number Gr and the Prandtl number Pr, and as such it characterizes the competition between the driving thermal buoyancy and the damping viscosity and thermal diffusion. The higher the Rayleigh number is, the higher the convective intensity will be. We here calculate a Rayleigh number Ra $\sim 10^{11}$ for Nyiragongo lava lake, which greatly exceeds the critical value of $\sim 10^3$ required for convection to occur (e.g., Carrigan, 1987), highlighting the intense convective regime of the lava lake. This value is higher than that computed at Erta Ale lava lake (10^5–10^9, Harris, 2008), suggesting a more vigorous convective regime at Nyiragongo.

The Reynolds number Re is defined as the ratio between inertial and viscous forces within a fluid, and is used to indicate whether the flow is laminar ($Re < 2200$) or turbulent (e.g., Turcotte and Schubert, 2002). We here calculate a Reynolds number Re $\sim 10^2$, well below the critical value of $\sim$2200, suggesting that the flow is laminar. This implies that viscous forces in the lake are dominant with respect to the inertial forces, and can explain why the observed surface flow is characterized by a smooth and fairly constant motion, rather then a turbulent motion which would tend to produce chaotic vortices. Low Reynolds number are also reported at Erta Ale ($Re = 10^{-1}$–10^2; Harris, 2008). At Nyiragongo however, Burgi et al. (2014) assume higher values ($Re > 10^4$) in order to explain the system's ability to drain large magma volumes in short periods. These likely represent upper-end estimates, which are more representative of the fluid at greater depths where viscosities reach very low values (i.e., 60 Pa·s, Giordano et al., 2007). Moreover, sudden lake level drops could also be caused by sudden gas release from the lake rather than by magma drainage into the conduit, in which case lower Reynolds values could be expected.

Lastly, we calculate the Prandtl number Pr, defined as the ratio between kinematic viscosity and thermal diffusivity, and the Nusselt number Nu, defined as the ratio between total heat flux and heat flux in a purely conducting regime. While Prandtl number gives information on the ability of the fluid lava lake to transfer its kinetic energy in thermal energy, the Nusselt number measures the relative importance of convective heat transport compared with the total heat flux (Anderson, 2007). We found that while Prandtl number is high Pr $\sim 10^4$, the Nusselt number is very low $Nu < 10^2$, both indicating that convection is very effective in transferring energy in comparison to conduction, which is meaningful in systems affected by vigorous convection. Similar values are reported at Erta Ale lava lake (Pr $\sim 10^4$–10^5, Harris, 2008).

4.5. Spatter cone transition from explosive to effusive activity

The volcanic activity of the new vent was intermittent, and our infrasonic record shows (Fig. 8b–c) that during the 2-day campaign activity alternated between: (i) periods of intense explosive activity, characterized by impulsive transients with high pressure amplitude (reaching 15 Pa, e.g. on 2016-04-20 11:00–18:30 GMT), (ii) periods of intense infrasonic activity but without any explosive events (e.g., from 2016-04-20 18:30 GMT till 2016-04-21 08:30 GMT), and (iii) periods of relative quiescence, characterized by low pressures (<2 Pa, e.g. on 2016-04-21 11:00–13:00 GMT).

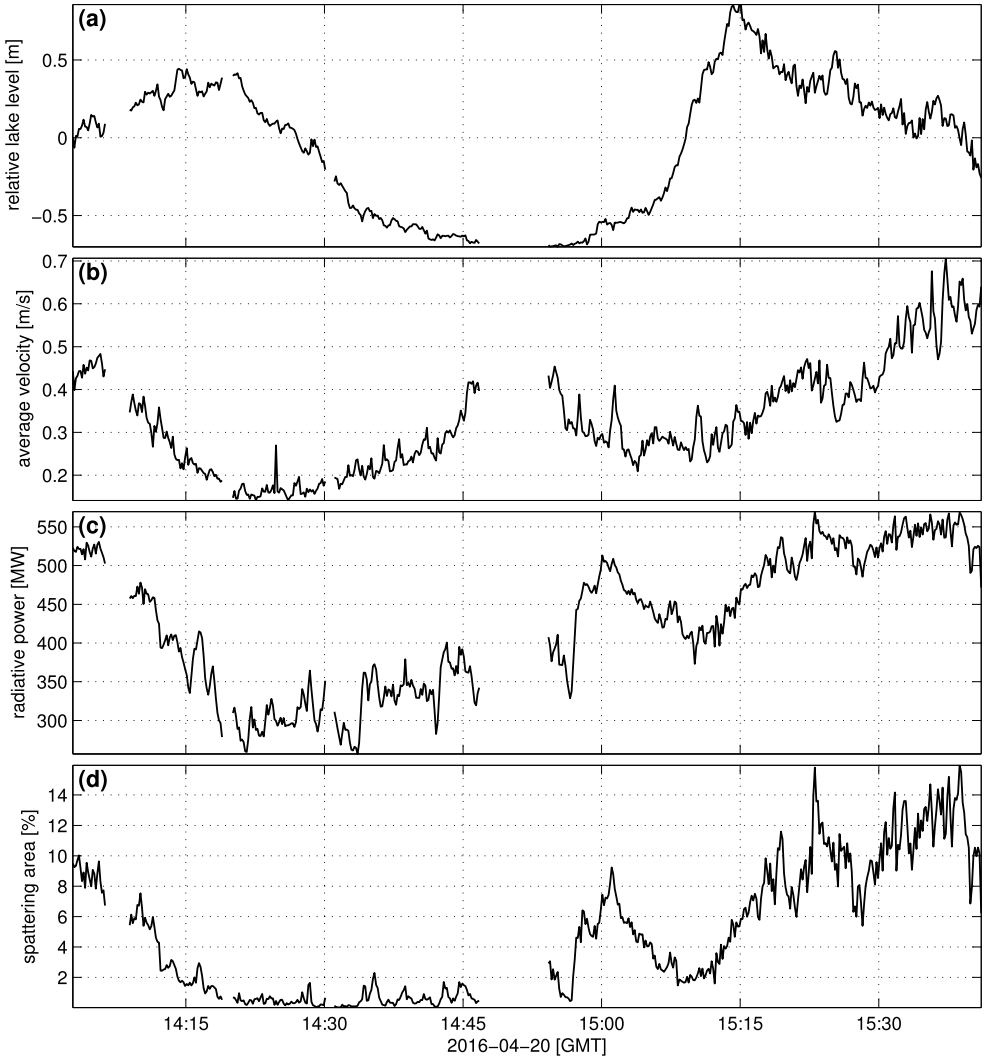

Fig. 7. (a) Lake level variation (see Supplementary Video 6), (b) average lake surface velocities, (c) lake radiative power, and (d) degassing intensity, estimated as the percentage of the lake surface affected by spattering.

Array analysis reveals that coherent infrasonic signal comes from two distinct directions centered around 26°N and −4°N (Fig. 8d), corresponding respectively to the direction of the new spatter cone and of the lava lake (blue and red markers respectively). Pressure amplitudes indicate that the spatter cone is the source of stronger infrasonic signal, reaching maximum amplitude of 15 Pa compared with 1.3 Pa for the lava lake (Fig. 8c). Although the infrasonic activity of the lava lake is fairly stable through time in terms of amplitude and persistence, the spatter cone activity varies significantly, switching between (i) phases of quiescence, (ii) explosive activity, and (iii) effusive activity.

The onset of the explosive activity (identified by orange markers in Fig. 8a) is sharp. The number of transients increases up to a stable rate of ∼100 events / 5-min in a very short time, while infrasonic pressure reaches values >10 Pa in a few minutes. This infrasonic activity typically lasted from 2.5 to 8 hr. At the beginning of this phase, the infrasonic transients are associated with loud explosions, rich in gas and with no ejection of magma fragments. Progressively, explosions become richer in fresh lava clots and less violent, as evidenced by the waning trend in the infrasonic amplitudes. Eventually, this explosive activity shifted towards an effusive regime (identified by green markers in Fig. 8a), during which explosions became nearly continuous, forming a sustained jet several meters high. Magma then overflows from the cone, feeding a lava flow which spreads onto platform P3 before cascading into the lava lake (Supplementary Video 1). The transition from explosive to effusive regime is very clear on the infrasonic record, as the large infrasonic transients associated with single explosions become smaller and more frequent (Fig. 8a). This pattern closely recalls the transition from strombolian- to hawaiian-type activity, where it is thought that increasing gas flux in the conduit causes the transition from a slug-flow to a churn-flow (Taitel et al., 1980; Ulivieri et al., 2013).

The first effusive phase lasted 16.5 hr, while the second was not over when the recording campaign ended, 8 hr after its start. During effusive periods, there were almost no infrasonic detections coming from the lava lake, as its activity was most likely masked by the larger infrasonic energy generated by the spatter cone. Indeed, as soon as the effusion rate decreased, the number of detections coming from the spatter cone decreased, and the array started to pick up signals from the lake once again (i.e., at 09:00 GMT, 2016-04-21).

Rough estimations of the effusion rates were obtained from visible camera recordings taken on April 21. We first estimated the surface velocity of the flow as it traveled down the cone, using the Farnback optical flow algorithm. This surface velocity was then converted to mean flow velocity, taken as 2/3 of the maximum surface velocity when the channel cross-section is considered rect-

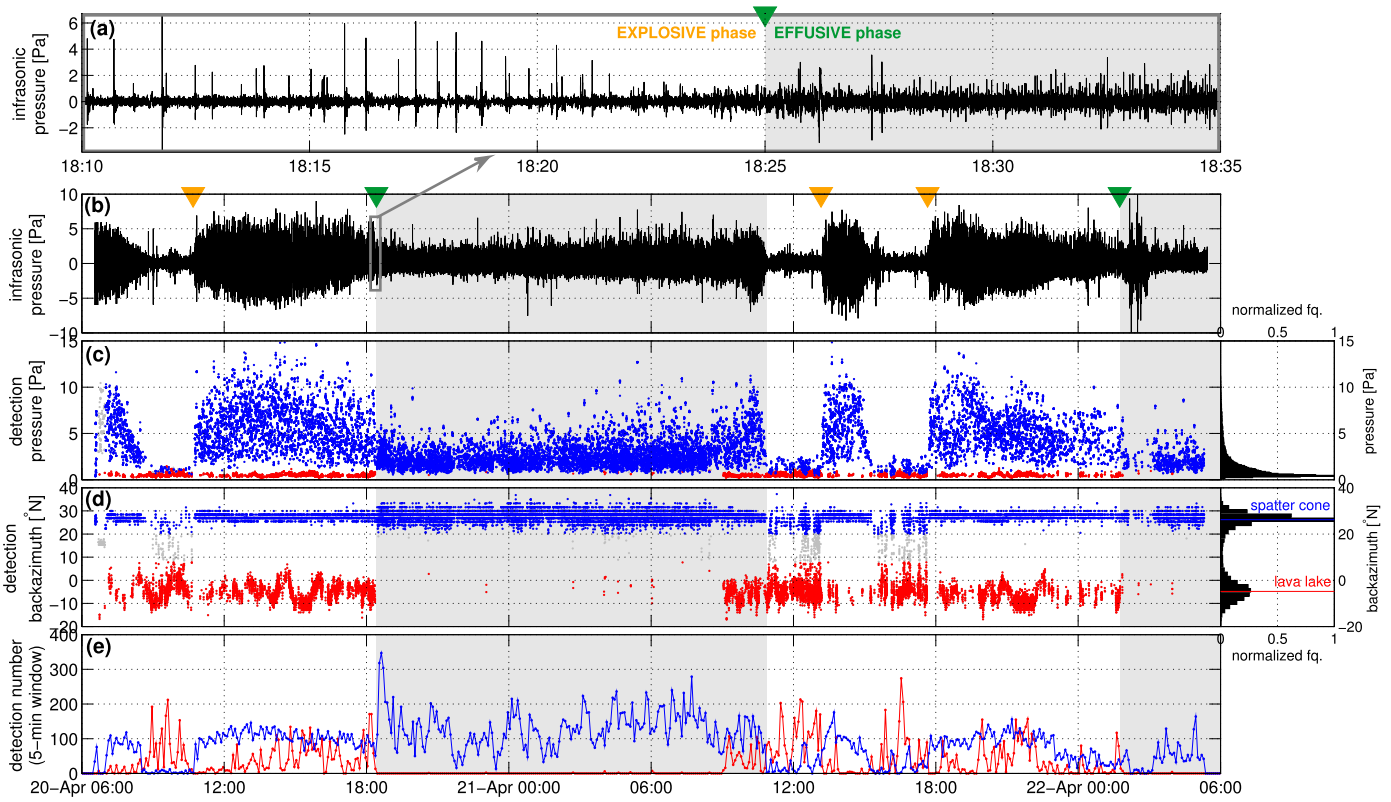

Fig. 8. Infrasonic trace band-passed filtered between 0.5–10 Hz, (a) zoomed during the transition from explosive to effusive activity, and (b) throughout the entire field campaign. Result of the infrasound array analysis by multichannel semblance: (c) infrasonic pressures originated by the spatter cone (blue markers) and the lava lake (red markers), (d) back-azimuth of the infrasonic detections, indicating two distinct directions centered around 26°N (spatter cone, blue markers) and −4°N (lava lake, red markers), (e) number of detections from the spatter cone and lava lake in 5-min windows. The orange triangle markers in plot (b) indicate the onset of the explosive activity, and the green markers the onset of the effusive activity. The effusive activity periods are shadowed in gray.

angular (Harris et al., 2007). Finally, supposing a channel depth and width of ∼1 m yields an effusion rate of ∼13 m^3/s. Over an 16-hr period, this yields a total of 0.75 Mm^3 of lava drained out the vent during a single effusive episode. During these effusive events the lava lake level did not vary significantly.

5. Discussion

5.1. Convective system and outgassing mechanism

Lake surface dynamics appears to be controlled by two processes (Fig. 9a): 1) upwelling, where crust is generated and spreads radially to accommodate the arrival of new magma from depth; and 2) downwelling, where crust is consumed as it is dragged into a region of persistent bubble bursting (spattering). The observed horizontal motion is thus likely to be the horizontal adjustment between rising and falling vertical currents of fluid magma. Although these vertical currents are driven by buoyancy, due to the gravitationally unstable state of the thermal boundary layer (TBL), the horizontal motion is in fact explained by a horizontal pressure gradient, as predicted by basic thermal convection theory in fluids (e.g., Bercovici et al., 2015). Indeed, on one hand the hot upwelling gas-rich fluid rising towards the surface induces a high-pressure region, pushing material away from the upwelling center. On the other hand, the cold downwelling degassed fluid tends to sink, generating a low-pressure region as it pulls away from the surface. Thus, the surface flow follows a pressure gradient, from high pressures above the upwelling center towards low pressures over the downwelling center. Such horizontal pressure gradient is the primary force driving the horizontal motion of thermal boundary layers in convective cells (Bercovici et al., 2015). Because the lake surface is deformable, this pressure gradient is expected to result in a topography gradient, where the upwelling center is a topographic high due to the hotter buoyant rising material, and the downwelling center is a topographic low where the cold dense material sinks. While local depression around the sinks can be observed from close-up photographs, the topographic high is not clearly visible, most likely because it is more widespread. Patrick et al. (2016b) however report lidar measurements at Kilauea lava lake, where they found the upwelling area to be 0.6 m higher than the downwelling area, subsequently suggesting that the topographic gradient between the two could sustain the observed surface flow. We build upon these findings and suggest that the flow follows a pressure gradient, which is also likely responsible for the observed velocity gradient.

The regions where plates converge behave as sinks, where violent spattering takes place. These likely correspond to the sites where the thermal boundary layer sinks into the lake as a cold downwelling plume (Fig. 9b), a phenomena also referred to as the “dripping” of negatively buoyant material (Harris, 2008). In their immediate vicinity, the surrounding crust appears to be pulled, and subsequently torn and consumed by chaotic bubble bursting. On a wider scale, the small bubbling spots which regularly appear near upwelling regions are carried by lake currents (Fig. 9b), and their trajectories trace curved paths across the lake surface which closely recall the helicoidal motion of a fluid being drained in a sink. As these sources get closer to the main downwelling site, they merge into long linear alignments and spattering becomes more vigorous. Similar observations have been reported by Perret (1913a, 1913b) at Kilauea, who noted that the region where lava rises is “highly charged with tiny fountains”, which are carried by the circulation of the lava, aka “traveling fountains”. As pointed out

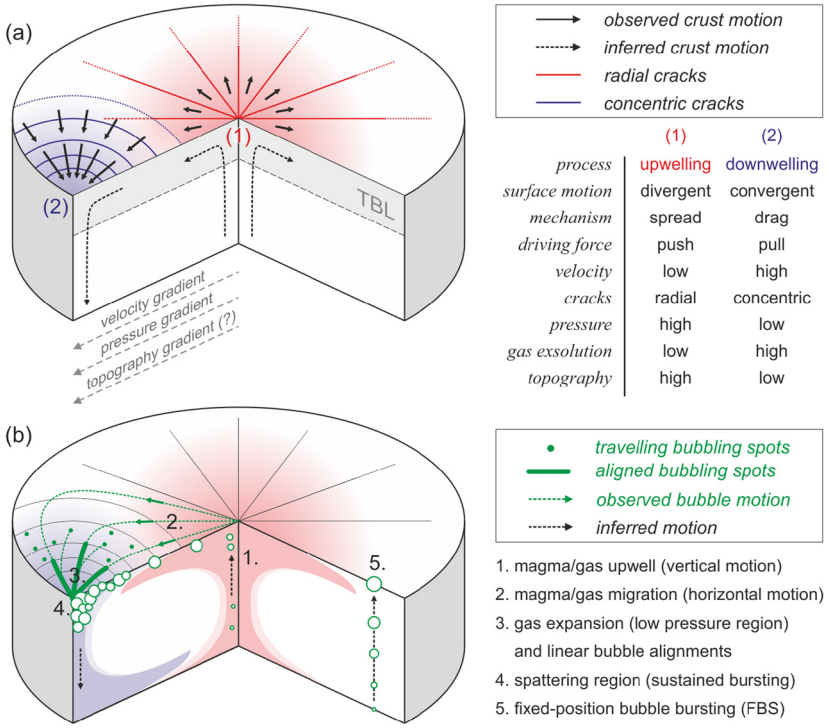

Fig. 9. Conceptual model of the lava lake convective system and outgassing mechanisms. (a) Observed surface motion, plate organization, and implications. TBL stands for thermal boundary layer, and refers to a transition region where the gravitationally unstable material is confined, between the top cold boundary and the more homogeneous lake interior (e.g., Bercovici et al., 2015). (b) Observed spattering dynamics and implications.

by Patrick et al. (2016a), these observations suggest that spattering is a shallow rooted mechanism.

The concentration of spattering in areas where plates converge (i.e., areas of lava downwelling, never upwelling), is similar to observations at both Kilauea (Patrick et al., 2016b, 2018) and Erta Ale (Harris et al., 2005), pointing to a generic aspect of lava lake dynamics. Gas concentration in a location of magma downwelling remains nonetheless rather counter intuitive. Two mechanisms could explain such feature. Firstly, the low pressures expected in downwelling regions could enhance gas exsolution in the shallow layer of magma beneath the crust, and thereby explain the high concentration of scattered bubbling spots. Volatiles exsolve from magma at different pressures (depths), and in a solubility hierarchy typical of basaltic systems, HCl and HF are the most soluble. However, although these are thought to be released at shallow depths (Sawyer et al., 2008), it is still unclear whether the low pressure conditions described here could significantly affect degassing in the lake. Secondly, the surface currents likely concentrate a shallow layer rich in small gas bubbles around the sink, which may eventually coalesce and thereby fuel the observed spattering. This mechanism, whereby spattering results from the release of large coalesced bubbles, is similar to that described by Patrick et al. (2016a) at Kilauea, but differs from the observations of Bouche et al. (2010) at Erta Ale, which interpret the lava fountains as the result of bubble clusters rising directly from the feeding conduit. These fountains however, have characteristics which differ significantly from the spattering described here (i.e., fixed position and duration ~90–120 s, compared to the persistent and constantly moving spattering sites), which suggest that these are distinct phenomena with different source mechanisms.

It is important to stress that at Kilauea, rockfalls into the lake are reported to trigger spattering, and subsequently create a new downwelling area that pulls the surrounding crust into it (Patrick et al., 2018). Although the small rockfall recorded during our campaign did not create a new downwelling site, we emphasize that in some cases spattering can be the initial driver for local plate motion. Perret (1913b) also reported how spattering sources influence the lava lake surface motion, and recognized that these are usually areas of lava downwelling. He explains this finding as the result of a "siphoning" effect, whereby the bursting of gas bubbles creates void space forming a local topographic depression that surrounding lava plunges into.

We also report evidence for a deeper source of gas, where gas bubbles rise independently of the convective cells and burst in a stationary position (labeled FBS in Fig. 3). This phenomenology is very similar to the sporadic "northern bubble bursts" described by Patrick et al. (2018) at Kilauea. Because it coincides with a region of lava upwelling, the authors suggest that such bubbles represent gas slugs traveling directly upward the conduit feeding Kilauea's lava lake. At Nyiragongo however, this fixed bubbling spot does not coincide with a zone of stable upwelling, therefore linking it to the feeding conduit is not so straightforward. Nonetheless, the fact that position of bubbling is stable regardless of the surface motion indicates in our opinion a stationary deep source of gas, from where gas bubbles rise following a vertical path. This has in turn two possible implications: (i) the lake has a shallow depth (at least in the peripheral regions), preventing the bubbles drifting laterally with deep circulations as it rises to the surface, and/or (ii) only the uppermost part of the lake is subject to strong lateral motion, and is not representative of the lake's interior motion. This second case was referred to as a "decoupled surface flow" by Patrick et al. (2016b), whereby the lava crust would only skim across the surface as a superficial layer, bearing no information on any underlying circulation in the lake.

5.2. Lake level and velocity fluctuations

Lake level fluctuation was recorded, in the order of 1.5 m in 1 hr. Such cyclic, meter-scale changes have long been reported at Nyiragongo (e.g., Tazieff, 1966; Spampinato et al., 2013), but only recently have been accurately recorded and attributed to gas piston activity (Smets et al., 2016). Gas pistoning is a phenomenon

which has been reported at several lava lakes. Three models have been proposed to explain this behavior: 1) periodic rise and burst of deep sourced gas slugs (Vergniolle and Jaupart, 1990), 2) periodic gas accumulation and release within or below the crust (e.g., Swanson et al., 1979; Patrick et al., 2016a), and 3) periodic lake recharge from a deeper reservoir due to varying magmastatic pressure (e.g., Witham et al., 2006). However, the gas slug driven model does not agree with the stability of the gas plume composition recorded by Sawyer et al. (2008) at Nyiragongo, and it has to be discarded. On the contrary, the model involving gas accumulation under the crust has instead been considered to be more appropriate for Nyiragongo (Smets et al., 2016). However, although there is convincing evidence that shallow gas accumulation trapped as a foamy layer drives the gas piston behavior at Kīlauea's lava lake (Patrick et al., 2016a), our data do not directly support this model. Indeed, we do not observe any clear "trapping" process, whereby the rise phase of the lake level would be associated with decreasing degassing activity (estimated here as the percentage of the lake occupied by spattering activity, Fig. 7d), and vise-versa during the falling phase. Moreover, unlike Kilauea volcano, small rockfalls inside the lava lake do not trigger any particular change in the spattering activity (e.g. at 11:38:48 GMT in Supplementary Video 2), suggesting that Nyiragongo's lava lake may not have such a well-developed superficial foam layer. This could be the consequence of the higher plate velocities, which result in smaller plates and thus more permeable crust then at Kilauea. It is also unclear whether the dynamic pressure balance model (Witham et al., 2006) could apply to explain the observed data. Indeed, although the timing of the lake level variations with respect to the plate velocities and the gas release seems more appropriate (e.g., gas release appears to diminish during the fall phase and to increase during rise phase), the relationship is not straightforward. In addition, it is unclear weather such small fluctuations (∼1 m) can affect the magmastatic pressure of a shallow reservoir.

It is possible that neither of these models is entirely flawed, and that either or both might operate under different starting conditions. Moreover, it should be considered that the magma exchange between the cold sinking degassed magma, and the hot rising gas-rich magma can be pulsatory (Huppert and Hallworth, 2007). Such bi-directional flow in the conduit feeding the lava lake has been invoked to explain the spectacular oscillations of lake surface speed, temperature, and gas flux recorded at Erebus (e.g., Oppenheimer et al., 2009; Peters et al., 2014a). We stress that our video measurements are limited both in time and space (a portion of the lake is not visible in the field of view, preventing from a complete observation of the spattering sources). In order to better constrain the mechanisms driving such oscillations, future studies should focus on longer infrared recording periods, which should be coupled with infrasonic and gas flux measurements to quantify the outgassing activity.

Lastly, we report fluctuations of surface velocities with a minimum period of 80 s. Fluctuations in the lake surface velocity were also observed at Erebus lava lake, with a period of 5–18 min (e.g., Oppenheimer et al., 2009; Peters et al., 2014a, 2014b). These were shown to correlate with gas plume flux and composition, and were therefore explained as resulting from pulsatory magma supply into the lava lake, due to boudinage of the ascending magma flow within the conduit. The fluctuations reported here however have a higher frequency, and are less stable through time. Moreover, the lava lakes at Nyiragongo and Erebus are significantly different, in terms of magma viscosities (60–150 Pa·s and 10^4–10^8 Pa·s respectively), lake diameter (∼35 m and ∼200 m respectively), and feeding conduit geometry. Therefore, we cannot for now speculate on the appropriateness of such model to explain the observed velocity fluctuations. Longer observations are necessary to constrain the driving mechanism of these at Nyiragongo.

6. Conclusions

Nyiragongo volcano hosts one of the largest lava lake on this planet, threatening ∼1.5 million inhabitants in the surrounding area. It is of relative easy access, but only seldom has been the object of detailed geophysical studies. We here report for the first time a coupled analysis of thermal infrared footage and infrasound array recordings, which allowed to capture both the complex dynamics of the lava lake, and the eruptive activity of the internal eruptive vent opened early 2016.

A conceptual model of the lava lake's convective system and outgassing mechanism is derived. We show that the lake surface is composed of a mosaic of crustal plates, which glide from regions of upwelling where crust is generated (i.e., radial spreading accommodating the arrival of deeper magma), to regions of downwelling where crust is consumed (i.e., concentric drainage of surrounding material). The surface flow is thus explained as the horizontal adjustment between rising and falling vertical currents of magma, which effectively follows a horizontal pressure gradient between the high-pressure region (i.e., hot upwelling fluid impinging on the surface) and low-pressure region (i.e., downwelling fluid pulling away from the surface). Gas bubbles rise with the ascending hot magma, appearing near upwelling regions before being progressively dragged into downwelling regions. These latter regions act as a sink draining their surrounding environment, as suggested by the helicoidal trajectories of the gas bubbles traveling across the lake surface. The surface flow may thus concentrate in this region a shallow layer rich in small gas bubbles, which could coalesce and thereby fuel the persistent chaotic bubble bursting (i.e., spattering activity). This mechanism, whereby spattering represents the release of large coalesced bubbles, is similar to the description of Patrick et al. (2016a) at Kilauea. Such spattering activity, which is evidently shallowly rooted, is the main source of infrasound from the lake. We show how infrasound recordings can be used as a direct measure of the lake outgassing activity, whose intensity and position can be tracked using array analysis. Fluctuations of this outgassing activity have been continuously recorded throughout the entire recording campaign, but have not been clearly correlated with the oscillations of the lava lake level and of the surface speed, both detected by thermal video analysis. Future studies should undertake continuous video recordings spanning several days, coupled with infrasound array recordings in order to address these correlations adequately.

The eruptive activity of the internal eruptive vent opened 2016 was found to be intermittent. The infrasound array analysis clearly shows the transition from explosive to effusive regime: the first is characterized by large infrasonic transients associated with single explosions, while the second is characterized by smaller nearly continuous transients associated with a sustained lava jet. This pattern is typical of the transition from strombolian to hawaiian activity, which is thought to reflect increasing gas flux in the conduit. This lead magma to overflow from the cone, feeding a lava flow spreading onto platform P3 before cascading into the lava lake. The eruptive cycles of this new eruptive vent did not seem to affect significantly the activity or level of the lava lake. However the rarity of such phenomena at Nyiragongo can only call for increased monitoring attention, as it may reflect increasing overpressures in the shallow reservoir.

Our study constrains diverse aspects of the convective and outgassing dynamics at lava lakes, complementing and expanding observations reported elsewhere. These results not only provide quantitative observations for improved lava lake models, but also provide insights into the hidden mechanisms operating inside the shallow plumbing system at other open-vent mafic volcanoes.

Acknowledgements

We wish to thank Matthew R. Patrick, an anonymous reviewer, and the editor Tamsin Mather for their valuable suggestions which helped improve the manuscript. We are very grateful to the Goma Volcano Observatory Director for his invitation and logistic help, as well as the OVG staff which provided information on the activity of Nyiragongo. MONUSCO is warmly thanked for the great support in the field deployment by helicopter. The ICCN provided the logistic inside the National Parc of Virunga and provided full assistance with their rangers in the field. Special thanks to Francesco Pandolfo and Gabriele Erba for priceless support in the organization of the campaign and descent into the crater. We also wish to warmly thank Diego Coppola and Marco Laiolo for the fruitful discussions during preparation of the manuscript, as well as Matteo Cerminara for the discussions regarding the dimensionless analysis.

Appendix A. Supplementary material

Supplementary material related to this article can be found online at https://doi.org/10.1016/j.epsl.2018.08.004.

References

Anderson, D.L., 2007. The New Theory of the Earth. Cambridge University Press, Cambridge.

Arellano, S., Yalire, M., Galle, B., Bobrowski, N., Dingwell, A., Johansson, M., Norman, P., 2017. Long-term monitoring of SO_2 quiescent degassing from Nyiragongo's lava lake. J. Afr. Earth Sci. 134, 866–873. https://doi.org/10.1016/j.jafrearsci.2016.07.002.

Balagizi, C.M., Yalire, M.M., Ciraba, H.M., Kajeje, V.B., Minani, A.S., Kinja, A.B., Kasereka, M.M., 2016. Soil temperature and CO_2 degassing, SO_2 fluxes and field observations before and after the February 29, 2016 new vent inside Nyiragongo crater. Bull. Volcanol. 78 (9), 64. https://doi.org/10.1007/s00445-016-1055-y.

Ball, M., Pinkerton, H., 2006. Factors affecting the accuracy of thermal imaging cameras in volcanology. J. Geophys. Res., Solid Earth 111, 1–14. https://doi.org/10.1029/2005JB003829.

Barrière, J., Oth, A., Theys, N., d'Oreye, N., Kervyn, F., 2017. Long-term monitoring of long-period seismicity and space-based SO_2 observations at African lava lake volcanoes Nyiragongo and Nyamulagira (DR Congo). Geophys. Res. Lett. 44, 6020–6029. https://doi.org/10.1002/2017GL073348.

Bercovici, D., Tackley, P.J., Ricard, Y., 2015. The generation of plate tectonics from mantle convection. In: Treatise on Geophysics, 2nd edition, pp. 271–318.

Bobrowski, N., Giuffrida, G.B., Yalire, M., Lübcke, P., Arellano, S., Balagizi, C., Calabrese, S., Galle, D.T., 2016. Multi-component gas emission measurements of the active lava lake of Nyiragongo, DR Congo. J. Afr. Earth Sci. 134, 856–865.

Bouche, E., Vergniolle, S., Staudacher, T., Nercessian, A., Delmont, J.-C., Frogneux, M., Cartault, F., Le Pichon, A., 2010. The role of large bubbles detected from acoustic measurements on the dynamics of Erta 'Ale lava lake (Ethiopia). Earth Planet. Sci. Lett. 295, 37–48. https://doi.org/10.1016/j.epsl.2010.03.020.

Burgi, P.Y., Caillet, M., Haefeli, S., 2002. Field temperature measurements at Erta'Ale lava lake, Ethiopia. Bull. Volcanol. 64, 472–485. https://doi.org/10.1007/s00445-002-0224-3.

Burgi, P.Y., Darrah, T.H., Tedesco, D., Eymold, W.K., 2014. Dynamics of the Mount Nyiragongo lava lake. J. Geophys. Res., Solid Earth 119, 4106–4122. https://doi.org/10.1002/2013JB010895.

Carbone, D., Poland, M.P., Patrick, M.R., Orr, T.R., 2013. Continuous gravity measurements reveal a low-density lava lake at Kīlauea Volcano, Hawai'i. Earth Planet. Sci. Lett. 376, 178–185. https://doi.org/10.1016/j.epsl.2013.06.024.

Carn, S.A., 2002. Eruptive and passive degassing of sulphur dioxide at Nyiragongo Volcano (D.R. Congo): the 17 January 2002 eruption and its aftermath. Acta Vulcanol. 14 (1–2), 1–11.

Carrigan, C.R., 1987. The magmatic Rayleigh number and time dependent convection in cooling lava lakes. Geophys. Res. Lett. 14, 915–918. https://doi.org/10.1029/GL014i009p00915.

Davaille, A., Jaupart, C., 1993. Thermal convection in lava lakes. Geophys. Res. Lett. 20, 1827–1830. https://doi.org/10.1029/93GL02008.

de Magnée, I., 1959. Première exploration géophysique du volcan Nyiragongo (Kivu). Bull. Séances Acad. R. Sci. O.-m. 3.

Evrard, P., 1960. La Mission géophysique du Centre national de Volcanologie au volcan Nyiragongo (1959). Bull. Séances Acad. R. Sci. O.-m. 6, 731–747.

Giordano, D., Polacci, M., Longo, A., Papale, P., Dingwell, D.B., Boschi, E., Kasereka, M., 2007. Thermo-rheological magma control on the impact of highly fluid lava flows at Mt. Nyiragongo. Geophys. Res. Lett. 34. https://doi.org/10.1029/2006GL028459.

Harris, A.J.L., 2008. Modeling lava lake heat loss, rheology, and convection. Geophys. Res. Lett. 35. https://doi.org/10.1029/2008GL033190.

Harris, A.J.L., Carniel, R., Jones, J., 2005. Identification of variable convective regimes at Erta Ale Lava Lake. J. Volcanol. Geotherm. Res. 142, 207–223. https://doi.org/10.1016/j.jvolgeores.2004.11.011.

Harris, A.J.L., Dehn, J., Calvari, S., 2007. Lava effusion rate definition and measurement: a review. Bull. Volcanol. 70, 1–22. https://doi.org/10.1007/s00445-007-0120-y.

Helz, R.T., Thornber, C.R., 1987. Geothermometry of Kilauea Iki lava lake, Hawaii. Bull. Volcanol. 49, 651–668. https://doi.org/10.1007/BF01080357.

Huppert, H.E., Hallworth, M.A., 2007. Bi-directional flows in constrained systems. J. Fluid Mech. 578, 95–112. https://doi.org/10.1017/S0022112007004661.

Karlstrom, L., Manga, M., 2006. Origins and implications of zigzag rift patterns on lava lakes. J. Volcanol. Geotherm. Res. 154, 317–324. https://doi.org/10.1016/j.jvolgeores.2006.01.004.

Komorowski, J.-C., Tedesco, D., Kasereka, M., Allard, P., Papale, P., Vaselli, O., Durieux, J., Baxter, P., Halbwachs, M., Akumbe, M., Baluku, B., Briole, P., Ciraba, M., Dupin, J.-C., Etoy, O., Garcin, D., Hamaguchi, H., Houlié, N., Kavotha, K.S., Lemarchand, A., Lockwood, J., Lukaya, N., Mavonga, G., de Michele, M., Mpore, S., Mukambilwa, K., Munyololo, F., Newhall, C., Ruch, J., Yalire, M., Wafula, M., 2002. The January 2002 flank eruption of Nyiragongo volcano (Democratic Republic of Congo): chronology, evidence for a tectonic rift trigger, and impact of lava flows on the city of Goma. Acta Vulcanol. 14, 27–62.

Le Guern, F., 1987. Mechanism of energy transfer in the lava lake of Niragongo (Zaire), 1959–1977. J. Volcanol. Geotherm. Res. 31, 17–31.

Oppenheimer, C., Lomakina, A.S., Kyle, P.R., Kingsbury, N.G., Boichu, M., 2009. Pulsatory magma supply to a phonolite lava lake. Earth Planet. Sci. Lett. 284, 392–398. https://doi.org/10.1016/j.epsl.2009.04.043.

Patrick, M.R., Dehn, J., Dehn, K., 2004. Numerical modeling of lava flow cooling applied to the 1997 Okmok eruption: approach and analysis. J. Geophys. Res. 109, 1–17. https://doi.org/10.1029/2003JB002537.

Patrick, M.R., Orr, T., Sutton, A.J., Lev, E., Thelen, W., Fee, D., 2016a. Shallowly driven fluctuations in lava lake outgassing (gas pistoning), Kilauea Volcano. Earth Planet. Sci. Lett. 433, 326–338. https://doi.org/10.1016/j.epsl.2015.10.052.

Patrick, M.R., Orr, T., Swanson, D.A., Lev, E., 2016b. Shallow and deep controls on lava lake surface motion at Kīlauea Volcano. J. Volcanol. Geotherm. Res. 328, 247–261. https://doi.org/10.1016/j.jvolgeores.2016.11.010.

Patrick, M.R., Orr, T.R., Swanson, D.A., Elias, T., Shiro, B., 2018. Lava Lake Activity at the Summit of Kīlauea Volcano in 2016. U.S. Geological Survey Scientific Investigations Report 2018-5008, 58 pp.

Perret, F.A., 1913a. The lava fountains of Kilauea. Am. J. Sci. 35, 139–148.

Perret, F.A., 1913b. The circulatory system in the Halemaumau lava lake during the summer of 1911. Am. J. Sci. 35, 273–282.

Peters, N., Oppenheimer, C., Killingsworth, D.R., Frechette, J., Kyle, P., 2014a. Decadal persistence of cycles in lava lake motion at Erebus volcano, Antarctica. Earth Planet. Sci. Lett. 395, 1–12. https://doi.org/10.1002/2014GC005399.

Peters, N., Oppenheimer, C., Killingsworth, D.R., Frechette, J., Kyle, P., 2014b. Correlation of cycles in Lava Lakemotion and degassing at Erebus Volcano, Antarctica. Geochem. Geophys. Geosyst. 15, 3244–3257. https://doi.org/10.1002/2014GC005399.

Platz, T., Foley, S.F., André, L., 2004. Low-pressure fractionation of the Nyiragongo volcanic rocks, Virunga Province, D.R. Congo. J. Volcanol. Geotherm. Res. 136, 269–295. https://doi.org/10.1016/j.jvolgeores.2004.05.020.

Ripepe, M., Marchetti, E., 2002. Array tracking of infrasonic sources at Stromboli volcano. Geophys. Res. Lett. 29, 33-1–33-4. https://doi.org/10.1029/2002GL015452.

Sawyer, G.M., Carn, S.A., Tsanev, V.I., Oppenheimer, C., Burton, M., 2008. Investigation into magma degassing at Nyiragongo volcano, Democratic Republic of the Congo. Geochem. Geophys. Geosyst. 9, 1–17. https://doi.org/10.1029/2007GC001829.

Smets, B., D'Oreye, N., Kervyn, M., Kervyn, F., 2016. Gas piston activity of the Nyiragongo lava lake: first insights from a stereographic time-lapse camera system. J. Afr. Earth Sci. 134, 874–887. https://doi.org/10.1016/j.jafrearsci.2016.04.010.

Spampinato, L., Ganci, G., Hernández, P.A., Calvo, D., Tedesco, D., Pérez, N.M., Calvari, S., Del Negro, C., Yalire, M.M., 2013. Thermal insights into the dynamics of Nyiragongo lava lake from ground and satellite measurements. J. Geophys. Res., Solid Earth 118, 5771–5784. https://doi.org/10.1002/2013JB010520.

Swanson, D.A., Duffield, W.A., Jackson, D.B., Peterson, D.W., 1979. Chronological Narrative of the 1969–71 Mauna Ulu Eruption of Kilauea Volcano, Hawaii. U.S. Geological Survey Professional Paper, vol. 1056, 55 pp.

Taitel, Y., Bornea, D., Dukler, A.E., 1980. Modelling flow pattern transitions for steady upward gas-liquid flow in vertical tubes. AIChE J. 26, 345–354. https://doi.org/10.1002/aic.690260304.

Tazieff, H., 1966. Etat actuel des connaissances volcan Niragongo (République Démocratique du Congo). Bull. Soc. Géol. Fr. 7, 176–200.

Tazieff, H., 1977. An exceptional eruption: Mt. Niragongo, Jan. 10th, 1977. Bull. Volcanol. 40, 189–200. https://doi.org/10.1007/BF02596999.

Tazieff, H., 1994. Permanent lava lakes: observed facts and induced mechanisms. J. Volcanol. Geotherm. Res. 63, 3–11. https://doi.org/10.1016/0377-0273(94)90015-9.

Tedesco, D., Vaselli, O., Papale, P., Carn, S.A., Voltaggio, M., Sawyer, G.M., Durieux, J., Kasereka, M., Tassi, F., 2007. January 2002 volcano-tectonic eruption of

Nyiragongo volcano, Democratic Republic of Congo. J. Geophys. Res., Solid Earth 112, 1–12. https://doi.org/10.1029/2006JB004762.

Turcotte, D.L., Schubert, G., 2002. Geodynamics. Cambridge University Press, Cambridge, U.K.

Ulivieri, G., Ripepe, M., Marchetti, E., 2013. Infrasound reveals transition to oscillatory discharge regime during lava fountaining: implication for early warning. Geophys. Res. Lett. 40, 3008–3013. https://doi.org/10.1002/grl.50592.

Vergniolle, S., Jaupart, C., 1990. Dynamics of degassing at Kilauea Volcano, Hawaii. J. Geophys. Res. 95, 2793. https://doi.org/10.1029/JB095iB03p02793.

Wauthier, C., Cayol, V., Kervyn, F., D'Oreye, N., 2012. Magma sources involved in the 2002 Nyiragongo eruption, as inferred from an InSAR analysis. J. Geophys. Res., Solid Earth 117, 1–20. https://doi.org/10.1029/2011JB008257.

Witham, F., Woods, A.W., Gladstone, C., 2006. An analogue experimental model of depth fluctuations in lava lakes. Bull. Volcanol. 69, 51–56. https://doi.org/10.1007/s00445-006-0055-8.